

GOES advanced sounder design study

W. E. Bicknell, J.P. Kerekes, and D. P. Ryan-Howard

Lincoln Laboratory, Massachusetts Institute of Technology
244 Wood Street
Lexington, MA 02173

ABSTRACT

Interim results of a current study on upgrading the geosynchronous operational environmental satellite (GOES) infrared (IR) sounder are presented. Considered are a 15 cm diameter telescope to reduce instrument size and weight, use of a Fourier Transform Infrared (FTIR) interferometer for high spectral wavelength resolution, a small detector focal plane array (FPA) operating at 65K, and combining the instrument with a microwave sounder. Retrieval performance improvement from the FTIR sounder is estimated.

1. INTRODUCTION

This is a report of some interim results from an on-going study being conducted at MIT Lincoln Laboratory. The study is examining IR sounding instruments to be employed on geosynchronous weather satellites in the early 2000 time period. The aim of the study is to determine sounder instrument designs and configurations that could improve performance and reduce cost. The purpose of this report is to describe a point design that illustrates some of the technical issues being considered.

Performance improvement could result from using a small, cooled FPA. The FPA would increase radiometric sensitivity as well as reduce time required for sounding a given geographical area. Combining the IR sounder with a microwave sounder would improve overall retrieval performance, particularly from cloud covered areas.

Cost could be reduced by utilizing smaller, less expensive boosters for launching satellite payloads into geosynchronous orbit. To accomplish this the current GOES payload consisting of an IR sounder, imager, and several other instruments might be separated into two packages. Figure 1 illustrates this concept where a microwave and IR sounder are on a separate satellite that is operated in close orbital proximity to a satellite for the imager and associated instruments. The idea is that of replacing a few large satellites with a constellation of smaller ones. This would lower individual launch costs and would also allow upgrading satellites with improved instrumentation on a less expensive and more timely basis.

Spacecraft weight savings may be achieved by using lightweight alloy structures, lithium batteries, and plasma thrusters. Weight savings could be achieved for an imager and an IR sounder by using lightweight optics and high density electronics packaging. Further weight reduction of an IR sounder might be achieved by utilizing a smaller telescope aperture than currently used.

Table 1 illustrates a weight budget for projected combined IR and microwave sounder.

Table 1. Projected Weight (lbs) of GOES Instruments

Instrument	Current	Advanced
IR Sounder	290	130
Microwave Sounder	-	220
Imager	270	-
Total Weight	560	350

This work was sponsored by the National Oceanic and Atmospheric Administration under Air Force Contract F19628-95-C-0002.

It is seen from Table 1 that a total weight reduction of about 200 lbs is sought. Combined with a possible, 150 lb weight reduction in the spacecraft, the total dry weight of an IR/microwave sounder could then be brought into the Delta 2 and Ariane 4 geosynchronous payload launch capability.

An estimate of the radiometric and retrieval performance that might be achieved with a geosynchronous IR sounder that is mated to a microwave sounder has been developed. The IR sounder point design employs a cryogenically cooled FPA and a 15 cm, rather than the current GOES 31 cm, telescope aperture diameter.

2. IR SOUNDING REQUIREMENTS

Next generation GOES sounding instrumentation should satisfy geosynchronous sounding requirements of the National Weather Service (NWS). Table 2 shows a summary of the required temperature and moisture sounding accuracy.¹ In addition to Table 1, requirements include the capability of sounding both a 3000 x 3000 km² synoptic scale area and a 1000 x 1000 km² mesoscale area in 60 minutes.

Table 2. Observational Accuracy Requirements (RMS Error)

Altitude Range	Temperature	Humidity	Vertical Resolution
Sfc-300 mb	1K	10%	1-2 km layers
300-100 mb	1K	20%	2-3 km layers
Above 100 mb	1K	-	3-6 km layers

The NWS will require high IR spectral resolution soundings with a resolution on the order of that achievable with FTIR, grating, etalon, or other relatively high-resolution interferometers.² Other high-resolution instruments will be examined before completion of the study. However, this report considers a point design for a compact FTIR interferometer of the type being developed for the GOES High-Resolution Interferometer Sounder (GHIS) brassboard.^{3,4}

3. MICROWAVE SOUNDER

There is a benefit from simultaneously combining geosynchronous IR sounding with microwave sounding.⁵ A microwave sounder has the capability to provide temperature and humidity profiles in the presence of clouds. Although not a major subject of this study, several aspects of a microwave design will be described to illustrate mating a microwave and IR sounder.

If a microwave sounder and IR sounder operate together, both will need to meet the NWS coverage rate requirements. This requirement is assumed to necessitate an hourly 45 minute synoptic scale coverage, a 5 minute mesoscale coverage, and an allowance of 10 minutes for IR calibration and satellite positioning.

A 2 meter antenna microwave sounder strawman design being considered by a geosynchronous microwave sounder working group study has been adapted to the NWS coverage and rate requirement.⁶ The operating frequencies are at 118 and 400 GHz for temperature sounding in oxygen bands and at 183 GHz for water vapor sounding. The 400 GHz frequency was chosen to provide high resolution with a 2m antenna with the knowledge that water vapor continuum absorption may prevent sounding below a few km altitude in the tropical latitudes. Table 3 shows a summary of the microwave sounder parameters.

Table 3. Microwave Sounder Parameters

Nominal Frequency (GHz)	118	183	400
Wavelength, λ , (mm)	2.54	1.64	0.75
IGFOV (Diam.) at 36,000 km (km)	60	38	18
IGFOVs in 3000 ² km ²	2600	6200	28000
IGFOV Integration Time, T_i (Sec)	1.1	0.43	0.10
Noise Temperature, T_N (K)	1000	1000	2000
ΔT_{rms} (K) BW: 100 - 400 MHz	0.1 - 0.05	0.15 - 0.08	0.64 - 0.32
Azimuth Scan Rate (Degrees/Sec)	0.09		

The instantaneous ground field of view (IGFOV) is evaluated over a 3000 km x 3000 km plane normal to the equatorial satellite projection axis as indicated in Figure 1. The plane subtends a 4.8 degree x 4.8 degree solid angle at the satellite. No spherical geometric projection factors have been used.

The 50% beam response IGFOV shown in Table 3 is given by

$$IGFOV = \frac{1.3\lambda}{D} \times 36000 \text{ km} \quad (1)$$

where D is the antenna diameter. The IGFOV integration time is then 45 minutes (2700 Sec) divided by the number of IGFOVs in 3000² km².

The receiver sensitivity, ΔT_{rms} , is given by

$$\Delta T_{rms} = \frac{T_N}{\sqrt{BW \times T}} \quad (2)$$

The front end mixer noise temperatures in Table 3 are projected values assuming about a factor of two reduction from those that are currently available. With this assumption, which is not considered unreasonably optimistic, a receiver sensitivity less than 1K would be achieved at all frequencies.

Since the IGFOVs of the three frequencies are different, it is assumed that the 183 GHz and 400 GHz IGFOVs are raster scanned over the larger, 60 km, 118 GHz IGFOV while all three are being scanned in azimuth. The raster scan might be achieved by scanning the antenna feeds. The overall azimuth scan rate is then given by the requirement of 50 (3000 km/60 km) azimuth scans over a 4.8 degree swath in 2700 seconds. The scan pattern is illustrated in Figure 2. One method for scanning the microwave antenna and IR sounder might be to scan the entire satellite using incremental braking and acceleration of sets of otherwise balanced momentum wheels.

4. INFRARED SOUNDER

A point design IR sounder is assumed to employ a small, 6 x 6 or 8 x 8, array of cooled HgCdTe photovoltaic detectors. Each detector will view an approximately 9 km diameter patch with a 10 km patch spacing. A scan pattern for obtaining a simultaneous microwave and IR sounding then becomes an issue.

4.1 Scan pattern

Figure 2 shows the IGFOV footprint of the 6 x 6 array co-aligned with the 118 GHz microwave sounder footprint. Figure 2 illustrates one mode of simultaneous operation of the two instruments. A turning flat in the IR sounder optical train will be used to counter-scan against the microwave azimuth scan, thereby holding the IR field of view (FOV) steady during an integration period. The counter-scan mirror will periodically be reset in step with the motion of the 118 GHz azimuth scan and the raster scan of the 183 GHz and 400 GHz receivers. For integration time estimates to be described, a 25 mSec counter-scan mirror reset time is assumed

4.2 Optics

The IR sounder optical train is assumed to be a re-imaging design similar to the current GOES, three-waveband sounder except that it, like GHIS, employs an FTIR interferometer rather than a filter wheel. The design is illustrated in Figure 3 for one waveband. A field stop at the telescope focus defines the overall field of view (FOV). A collimating mirror with its focus at the telescope focus collimates the incoming radiation and directs it into an FTIR interferometer. The collimating mirror images the entrance pupil at the Lyot stop that lies at the end of the FTIR interferometer working distance. A re-imaging mirror images the front field stop onto a set of microlenses. The diameter of the microlens defines the instantaneous field of view (IFOV) which, in turn, determines the IGFOV. Finally, the microlenses in combination with the re-imaging mirror image the Lyot stop onto each detector of the 65K FPA.

Figure 3 does not show two dichroic filters after the Lyot Stop that are used to separate the sounder into three waveband channels. And, although a detector bandpass filter and the microlens array should be cold, the cryogenic configuration is illustrative only. Figure 3 does contain notation for optical parameters for a point design described in Table 4.

Table 4. Point IR Sounder Optical Design Parameters

Design Parameters		Dependent Parameters	
IFOV (μ rad)	244	Collimator to Lyot Stop (cm), Sw	11
Diag. FOV (mrad), 6x6 Array	2.36	Lyot Stop Diameter (cm), D_{ls}	1.25
Entrance Pupil Diameter, (cm) D_p	15	IFOV Micro-Field Lens Diameter (mm)	1
Primary Mirror Focal Length (cm) f_p	120	FOV Micro-Field Lens Diameter (mm)	10
Collim. Mirror Focal Length (cm) f_c	10	Interferometer IFOV Angle (mrad)	3
Re-Image Mirror Focal Length (cm) f_r	35	Interferometer Diag. FOV Angle (mrad)	28.3
Micro-field Lens Focal Length (cm) f_m	0.14	Detector Focus Distance (mm), f_d	1
Primary to Entrance Pupil (cm) S_p	5	Detector Size (mm), Ddet	0.05

Table 4 describes a point optical design based on simple paraxial ray formulae. The design parameters in the left column determine the dependent parameters shown in the right column. The IFOV is the same as the current GOES filter wheel sounder. The 15 cm entrance pupil, is just less than one-half the current GOES sounder. An $f/8$ telescope with a 120 cm effective focal length, f_p , is indicated. This can be compared to the approximately 370 cm effective focal length of the GOES $f/11.9$ telescope.

A 10 cm focal length collimating mirror is indicated. This gives a 11 cm interferometer working distance, Sw, which is tight, but is similar to the compact GHIS brassboard design. The ratio of the telescope and the collimating focal lengths, f_p/f_c , gives a x12 magnification of the FOV angle for the FTIR interferometer working angle. This may be compared to a x36 magnification for the proposed GHIS system. This smaller magnification helps reduce self-apodization effects in the FTIR interferometer.

The microlens array employs 1mm individual lenses operating at $f/1.4$. A detector size of $50 \mu\text{m}$ is nominally matched to HgCdTe IR photovoltaic FPA sizes.⁷ The detector FPA and the microlens array are items that are not currently available. However, they are developable and within the range of current technology.⁸

The use of detector readout integrated circuits (ROICs) pose a challenge to timing requirements needed for accurate sampling of an interferogram.⁹ It is likely that a 6×6 HgCdTe photovoltaic array can be implemented with direct leads which will circumvent this issue. However, employment of an 8×8 or larger array may require ROIC development.⁸

Figure 4 shows a ray trace of an optical system based on the parameters of Table 4. The figure shows a two-element unobscured telescope. It also shows the use of a visible/IR beamsplitter to provide a visible image of the sounding that is used in retrieval. Figure 4 shows use of dichroics to divide the radiation into three wavebands.

It has been estimated that approximately 200 mW of cooling would be sufficient to obtain 65K operation of a thermally insulated bandpass filter, microlens, and 6×6 FPA. Required refrigeration for three wavebands might then be achieved with Stirling-cycle or pulse-tube cryocoolers that could maintain a 65K cold tip while providing a total of 600 mW of cooling. One refrigeration configuration that might achieve this is the employment of three miniature 250 mW, 65K cold tip pulse-tube cryocoolers.¹⁰ This refrigeration package would weigh about 20 lbs and require about 50 watts of electrical power. Isolation of the FTIR porch swing from the small, but finite, cryocooler vibration is an important consideration that remains to be investigated.

Detailed layout of the instrument depends on the supporting spacecraft design. However, Figure 5 is an artist's illustration of an instrument package. The illustration indicates use of a scanning mirror similar to the current GOES instrument. Also shown are two North-facing radiation coolers. One radiation cooler is used to maintain the optics interferometer at 220K, while the other radiates heat from the cryocooler refrigerator.

4.3 Radiometric performance

Detector sensitivity is a major issue, particularly for the longwave (LW) band. For a photovoltaic detector, the peak D^* is given by

$$D_{pk}^* = \frac{\frac{q\eta}{hc} \lambda_{pk}}{\sqrt{\frac{2kT}{R_d A_d} \left(\exp\left(\frac{qV}{kT}\right) + 1 \right) + 2\eta q^2 Q + \frac{[V_{na}^2] \exp\left(\frac{2qV}{kT}\right)}{(R_d)^2 A_d}} \quad (3)$$

where

- q = charge of an electron
- k = Boltzman's constant
- h = Planck's constant
- c = velocity of light
- η = quantum efficiency
- Q = detector photon flux
- T = detector temperature
- V_{na} = preamp noise voltage/ $\sqrt{\text{Hz}}$
- A_d = detector area
- R_d = detector zero-bias resistance
- V = detector bias (<0)

Figure 6 shows a plot of Eq.(3) for a peak D^* at 650 cm^{-1} using ambitious, but achievable, detector parameter values.⁸ The background flux, Q, assumed was based on calculations of 220K GHIS FTIR instrument NEAN.¹¹ The plot indicates that with modest bias at 65K, a peak D^* of 1.2×10^{12} can be obtained. This is within about 80% of BLIP. Also shown is a nominal photoconductive

HgCdTe peak D*. The use of the biased, 65K photovoltaic detector provides a gain of about x4 in sensitivity. This and other parameters assumed for the IR sounder are given in Table 5.

Table 5. Geosynchronous IR Sounder Performance Parameters (15 cm Aperture)

Band	Longwave		Midwave		Shortwave	
Wavelength (cm ⁻¹)	650 - 1150		1210 - 1740		2150 - 2721	
Spectral Resolution (cm ⁻¹), Δv	0.625		1.25		2.50	
Scene Flux (Ph/cm ² -Sec)	1 x 10 ¹⁶		1 x 10 ¹⁵		0.4 x 10 ¹⁴	
220K Instrument Flux (Ph/cm ² -Sec)	8 x 10 ¹⁶		6 x 10 ¹⁵		1 x 10 ¹⁴	
Total Detector Flux (Ph/cm ² -Sec), Q	9 x 10 ¹⁶		7 x 10 ¹⁵		1.4 x 10 ¹⁴	
65 K PV HgCdTe R _v A _d (Ohm-cm)	1.2		1000		10000	
Preamp Noise (Volt/√Hz), V _m	4					
Quantum Efficiency, η	0.7					
PV D _{pk} * (cm/Hz/Watt)	1.2 x 10 ¹¹		2.90 x 10 ¹¹		1.12 x 10 ¹²	
GHIS D _{pk} * (cm/Hz/Watt)	3.0 x 10 ¹⁰		1.37 x 10 ¹¹		1.07 x 10 ¹²	
<Diff Loss>/<GHIS Diff Loss>	0.93		0.96		0.98	
Detector Size (cm ²)	2.5 10 ⁻⁵					
GHIS Detector Size (cm ²)	3 x 10 ⁻⁵		6 x 10 ⁻⁵		7 x 10 ⁻⁵	
Focal Plane Array Size	6 x 6	8 x 8	6 x 6	8 x 8	6 x 6	8 x 8
Max. Self-Apodization Factor	0.993	0.987	0.996	0.993	0.997	0.996
Integration Time, T _i (Sec),	1.06	1.90	1.06	1.90	1.06	1.90
<NEDN> (mw/M ² -cm ⁻¹ -Sr)	0.80	0.60	0.16	0.12	0.05	0.03
GHIS Integration Time, T _{is} (Sec)	0.10					
GHIS <NEDN> (mw/M ² -cm ⁻¹ -Sr)	2.5		0.36		0.06	
Noise Factor	0.091	0.070				
GHIS Noise Factor	0.283					

Table 5 cites the wavebands and resolutions that are being used for the GHIS brassboard system. The Table indicates that the background flux on the detector is dominated by instrument radiation in the Longwave and Midwave bands. Decrease of the instrument temperature to below 220K is an option that might be considered. It would improve achievable sensitivity in all wavebands.

Diffraction loss contribution to an instrument transmission, τ, has been estimated. At 650 cm⁻¹ the geometric IFOV stop diameter lies just outside the second dark ring of the Airy function at the focus of the 31 cm GHIS system, giving a diffraction transmission loss factor of 91%.¹² For the 15 cm aperture system the geometric IFOV stop diameter (image of microlens diameter) lies

just at the first dark ring, giving a loss factor of 82%. The ratio of the loss factors of the 15 cm aperture to the 31 cm aperture is 0.9 at 650 cm⁻¹. Table 5 shows the ratio:

$$\frac{\tau_{diff}}{\tau_o} = \frac{\langle Diff Loss \rangle}{\langle GHIS Diff Loss \rangle}$$

where $\langle Diff Loss \rangle$ is an average over the waveband. The effect of diffraction on allowable IGFOV cross-talk is a subject to be further explored.

Interferometer self apodization has been considered.^{13, 14} The estimate uses an unpublished analysis of self-apodization developed at MIT/LL that employs Lommel functions.¹¹ The effects are small and are smaller in the Shortwave band than in the Longwave because of the decreased optical phase difference (OPD) used to achieve the required resolution.

For an FTIR interferometer system the noise equivalent differential radiance, NE ΔN , is given by

$$NE\Delta N = \frac{I}{A\Omega\tau\Delta\nu D^*} \sqrt{\frac{A_d}{T_i}} \quad (4)$$

where

- A = Entrance pupil aperture area
- Ω = IFOV solid angle
- τ = Optical transmission
- $\Delta\nu$ = Wavenumber resolution
- D* = Detector specific detectivity
- A_d = Detector area
- T_i = Integration time.

Equation (4) shows that reduction in entrance pupil aperture diameter increases the NE ΔN by the square of the reduction factor. The equation also shows that changes in optical transmission, τ , and in D* scale the NE ΔN by the ratio of the change, while increases in the integration time or decreases in the detector area decrease the NE ΔN by the square root of the ratio of the change.

Results summarized in Table 5 indicate that the combination of improvement in peak D*, increased integration time, and slightly smaller detector size is adequate to offset the approximately x4 increase in NE ΔN due to reduction in entrance pupil area and the effects of diffraction loss and self apodization. Further, the improvements appear sufficient to reduce the NE ΔN in each waveband to a value less than that for the 31 cm aperture GHIS system. For the LW band the improvement is most significant and critically depends on an improvement in the peak D*.

Results in Table 5 include a noise factor for the LW band which can be used to estimate the effects of improved NE ΔN on temperature retrieval error.

5. ESTIMATED TEMPERATURE RETRIEVAL ERROR

During the course of the GHIS effort, retrieval analysis simulations have been undertaken to estimate the performance improvement over the current GOES filter wheel sounder. The current simulations use a subset of TOVS Initial Guess Retrieval (TIGR) atmospheric profiles for training and a second, independent, TIGR set for statistically evaluating retrieval performance for a given set of GHIS waveband NE ΔN s.¹⁵

Analyses have shown that the temperature retrieval is most sensitive to the LW band NE ΔN . Providing NE ΔN s of the Midwave and Shortwave bands are not significantly different, changes in temperature retrieval error have been found to almost singularly depend on the LW $\langle NE\Delta N \rangle$. This has led to the development of a simple scaling factor applied to the LW band $\langle NE\Delta N \rangle$, called the noise factor, that can be used in predicting and describing results.¹⁶ A set of noise factor scaling results from recent retrieval

simulations has been made available and are used to estimate the improvement in temperature retrieval due to the projected improvement in $\langle \text{NEAN} \rangle$ suggested in Table 5. The results used are for a 1 km vertical resolution layer.

The noise factor, nf , is a scaling factor used for the effect of the LW band NEAN . It is given by

$$nf = \frac{\langle \text{NEAN} \rangle}{\langle \text{NEAN}_o \rangle} \sqrt{\frac{1}{NS}} \propto \frac{A_o \Omega_o \tau_o \Delta v_o D_o^*}{A \Omega \tau \Delta v D^*} \sqrt{\frac{1}{NS} \frac{A_d}{A_{do}} \frac{T_i}{T_{io}}} \quad (6)$$

where the notation has been previously described and the subscript "o" refers to a reference $\langle \text{NEAN} \rangle$ value used to compare one retrieval simulation to another. The factor NS is the number of number IGFOV sounding samples averaged. For a given ground cell size being evaluated by sounding, it is given by

$$NS = (1 - \text{Percent Cloud Cover}) \left(\frac{\text{Averaged Cell Size}}{\text{IGFOV Spacing}} \right)^2 \quad (7)$$

Typically, a 50% cloud cover is assumed for a 50 km cell size with a 10 km IGFOV spacing, giving $NS = 12.5$. For the IR sounder being considered compared to GHIS

$$\Omega_o = \Omega \Delta v_o = \Delta v$$

and

$$nf \propto \frac{A_o \tau_o D_o^*}{A \tau D^*} \sqrt{\frac{A_d}{A_{do}}} \sqrt{\frac{1}{NS} \frac{T_i}{T_{io}}} = \epsilon_f \sqrt{\frac{1}{NS} \frac{T_i}{T_{io}}} \quad (8)$$

The parameter ϵ_f reflects noise factor scaling due to fixed design parameters.

Figure 7 shows an estimate of the improvement in average RMS temperature error sounding provided by the 15 cm aperture, cooled photovoltaic FPA sounder. The temperature error is an average from 1000 to 300 mb. The GHIS temperature errors are from a study which predicted errors using an average over the TIGR data sets.¹⁶ The advanced sounder RMS sounder errors in Figure 7 were obtained by scaling the GHIS results using the improved noise factors shown in Table 5 that result from the lower LW $\langle \text{NEDN} \rangle$.

It is seen from Figure 7 that the projected performance is an improvement over the GHIS design, as expected. The temperature retrieval error also falls within the NWS requirement boundary. That the estimated error only "clips" or somewhat marginally falls within the boundary is not unexpected: It has been found in simulations that reduction in LW $\langle \text{NEAN} \rangle$ by a factor of 2 reduces the retrieved temperature error by approximately 20%. Also, it should be considered that the estimate here does not include improvement that will be derived from incorporating microwave sounding with the IR retrieval. In addition to a providing larger sounding measurement data base, the microwave sounder will greatly diminish the effect of cloud cover.

6. SUMMARY

This report describes interim results of an MIT/LL study on development of an advanced GOES IR sounder. The study is to explore possibilities for reducing cost and improving performance. A point design example has been given of a potentially smaller, compact IR sounder based on GHIS technology, lightweight, smaller aperture optics, and a 65K 6 x 6 or 8 x 8 photovoltaic HgCdTe FPA. The IR sounder operates with a microwave sounder housed in the same satellite. The example illustrates some of the issues encountered in providing an advanced geosynchronous sounder instrumentation system.

Results suggest that the retrieval performance from such a sounder system will be improved over the current GHIS design, will meet NWS requirements, and will provide soundings much less susceptible to cloud cover conditions.

Possible further improvement in IR performance might be achieved by operating the FTIR interferometer at a temperature lower than 220K. Operating the FPA at slightly higher than 65K temperature might be traded against a slightly larger aperture to arrive at an overall minimized weight.

It has been projected that the payload weight of such a combined microwave and IR sounder could be less than the current GOES series combined sounder and imager instruments. This invokes separation of the current imager and other instruments into a separate companion satellite. Interim results of ongoing studies of advanced IR and microwave geosynchronous sounders have been described. Final results on the merit and feasibility of a combined IR and microwave sounder instrumentation awaits the completion of both studies.

Technology that might be further pursued in preparation for development of an IR instrument includes LW photovoltaic HgCdTe FPAs, ROICs, microlens systems matched to such FPAs, and continued development of space-qualified cryocoolers.

7. ACKNOWLEDGEMENTS

In addition to those cited, the authors would like to acknowledge the contributions of W. M. Brown to the advanced sounder concept, D. L. Mooney for helpful technical discussions and critique, and D.E. Weidler for consultation on mechanical and thermal issues.

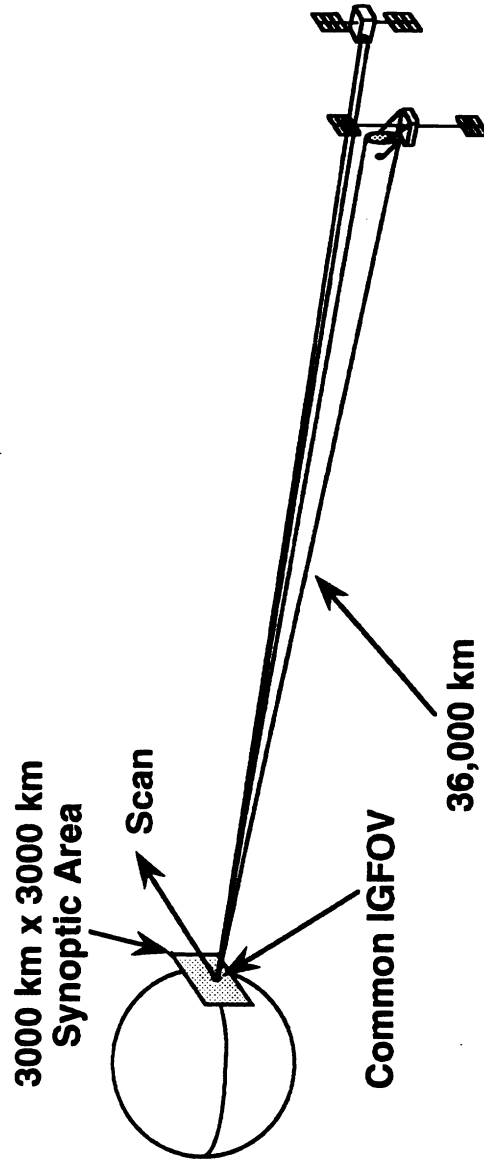
8. REFERENCES

1. National Oceanic and Atmospheric Administration, "National Weather Service observational requirements for the evolution of future NOAA operational geostationary satellites," Review Copy, 28 November 1995.
2. *ibid.*
3. W. L. Smith, et al, "GHIS-The GOES High-Resolution Interferometer Sounder," *Journal of Applied Meteorology*, 29, No 12, pp. 1189-1204, December 1990
4. Also see "Advanced Technologies and Instruments" in this Proceedings
5. D.H. Staelin and J.P. Kerekes, "Combined Microwave and Optical Atmospheric Remote Sensing Techniques: A Review," Proc. of 2nd Topical Symposium on Combined Optical-Microwave Earth and Atmosphere Sensing (CO-MEAS), April 3-6, 1995, pp. 3-6.
6. D. H. Staelin, Private Communication
7. E. E. Krueger, et al, "Extending HgCdTe Photovoltaic Detector Technology to Cutoff Wavelengths of 17 μm ," 1993 Spring Meeting of the Materials Research Society, San Francisco, CA, April 1993
8. M. Reine, Private Communication
9. L.M. Candell and D. M. Weitz, , "Electronics Considerations for a Geostationary Interferometer Sounder," to be published in this SPIE Proceedings
10. E. Tward, *et al.*, "Miniature Long-Life Space-Qualified Pulse-Tube and Stirling Cryocoolers," pp. 329-336, *Cryocoolers* 8, R.G. Ross, Jr., Editor, Proceedings of the 8th International Cryocooler Conference, Vail, Colorado, June 1994, Plenum Press, NY
11. D. R. Hearn, Private Communication
12. M. Born and E. Wolf, *Principles of Optics*, MacMillan, New York, 1964
13. R. J. Huppi, R.B. Shipley, and E. R. Huppi, "Balloon-borne Fourier spectrometer using a focal plane detector array," *Proc. Soc. Photo-Opt. Instrum. Eng.* 191, pp. 26-32, 1979

14. B.K. Yap, W. A. M. Blumberg and R. E. Murphy, , "Off-axis effects in a mosaic Michelson interferometer," *Applied Optics*, 21, pp. 4176-4128, November 1982

15. Allen Huang, Private Communication

16. W. L. Smith, Private Communication



**Geosynchronous Microwave and IR Sounder
(Two Satellite Constellation)**

Figure 1. Advanced sounder concept.

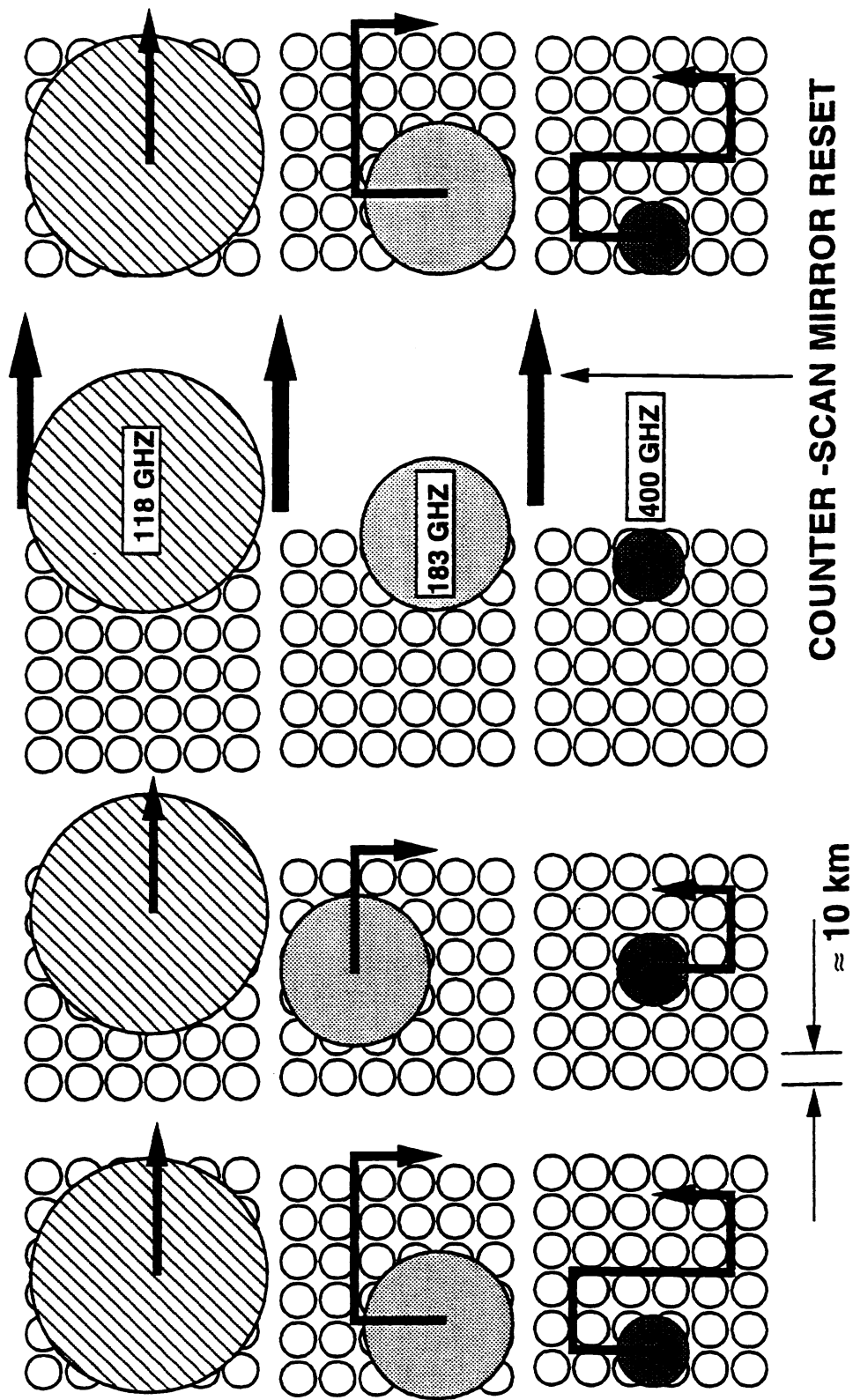


Figure 2. Microwave and IR scan pattern.

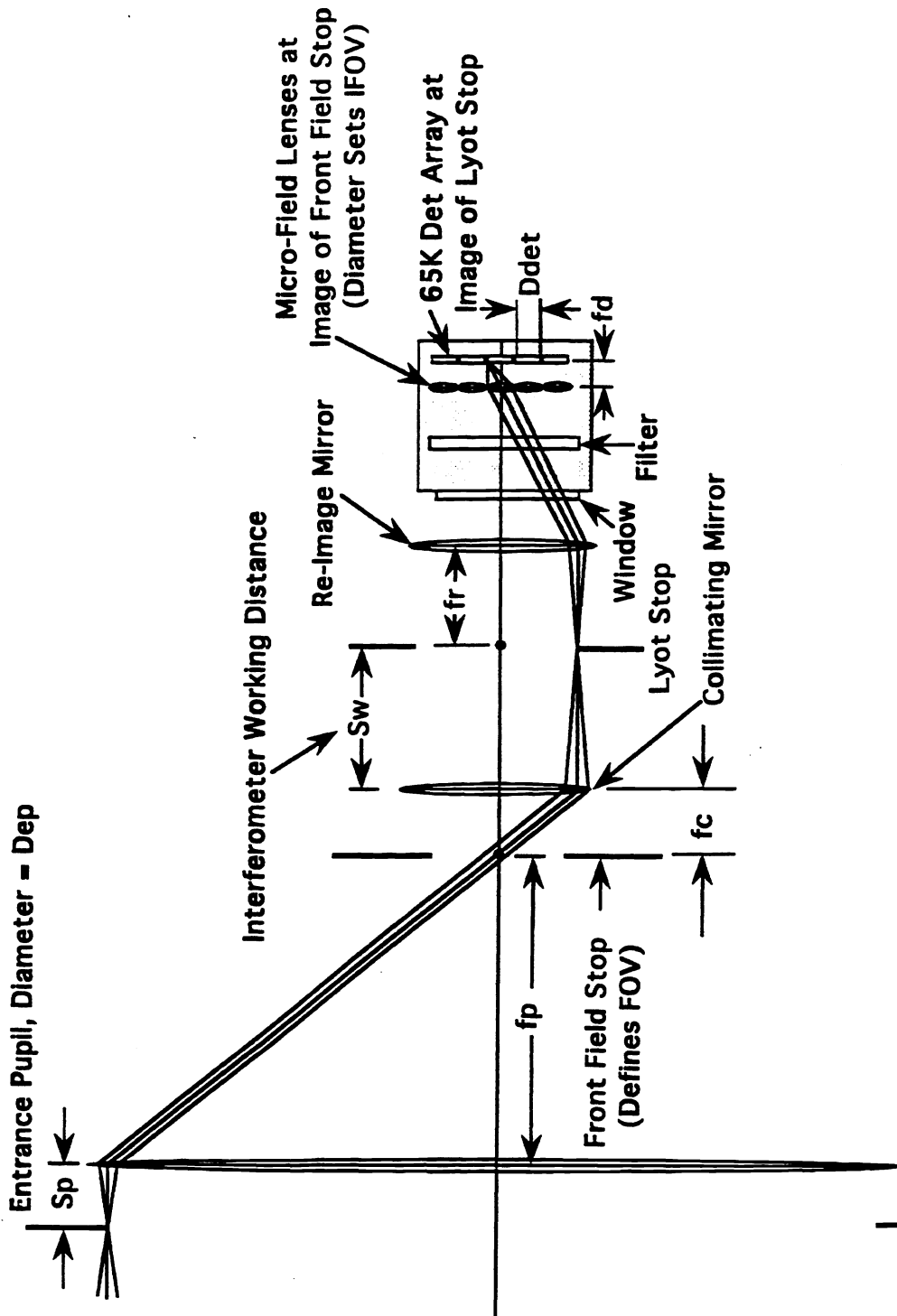


Figure 3. Schematic IR sounder optical design.

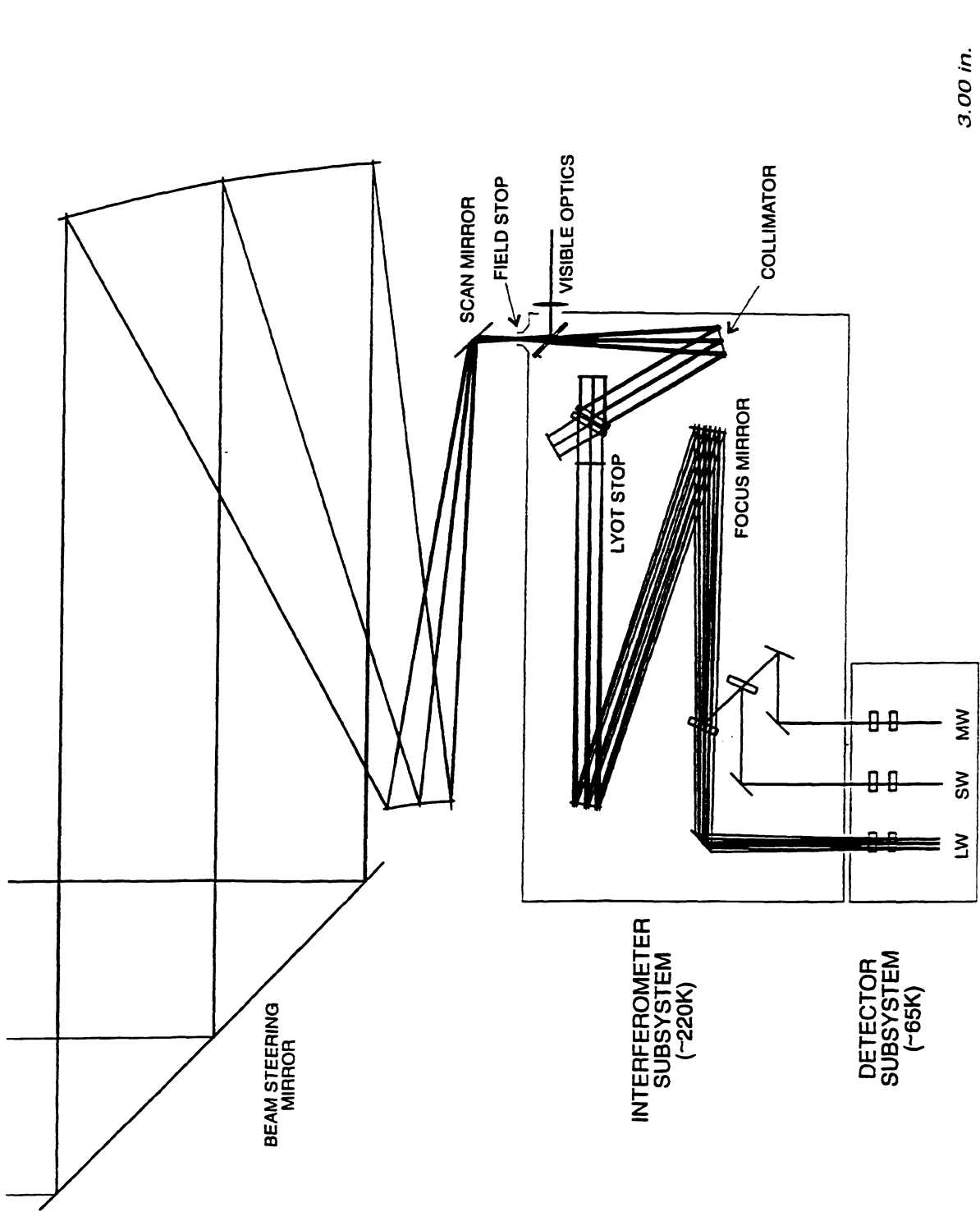


Figure 4. Ray trace and layout of IR sounder optics.

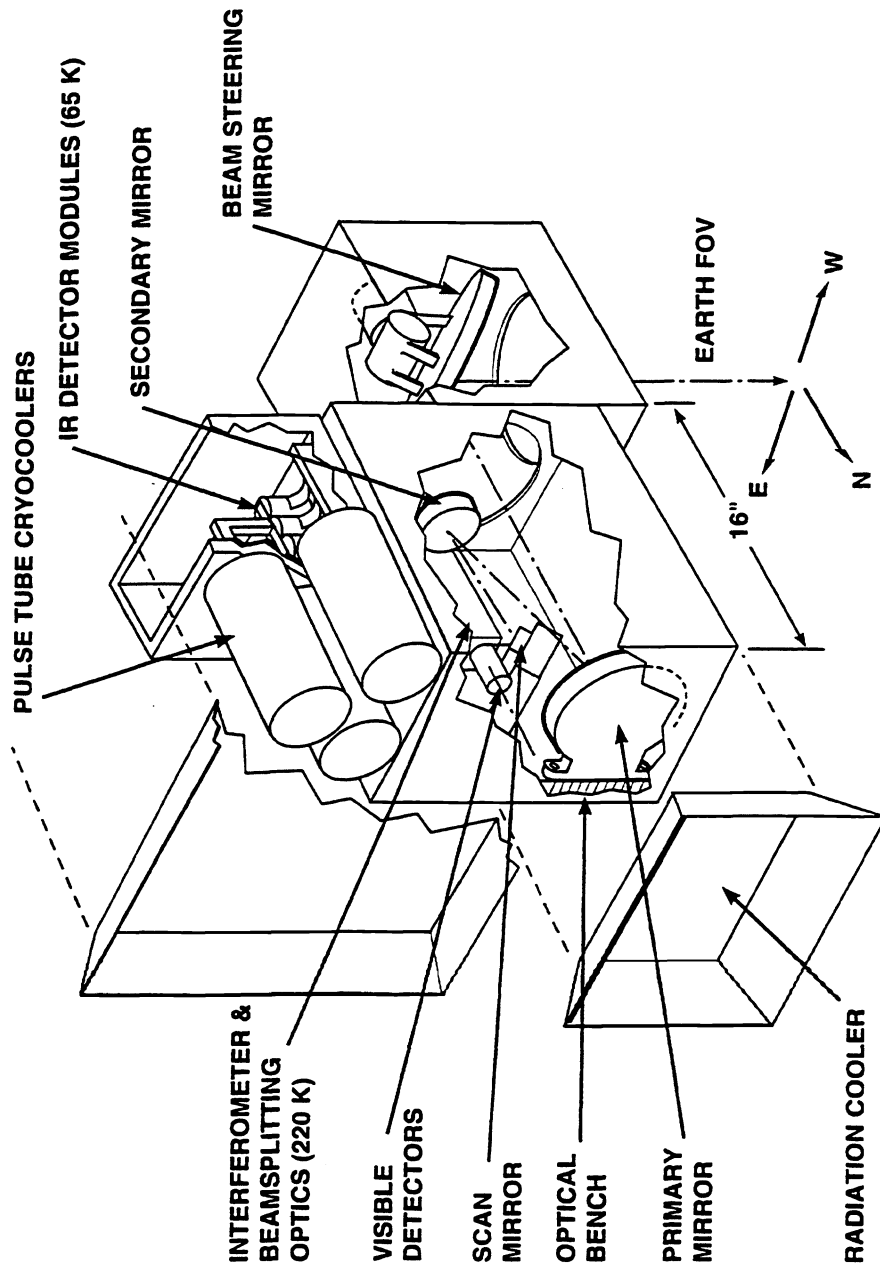


Figure 5. IR sounder instrument package.

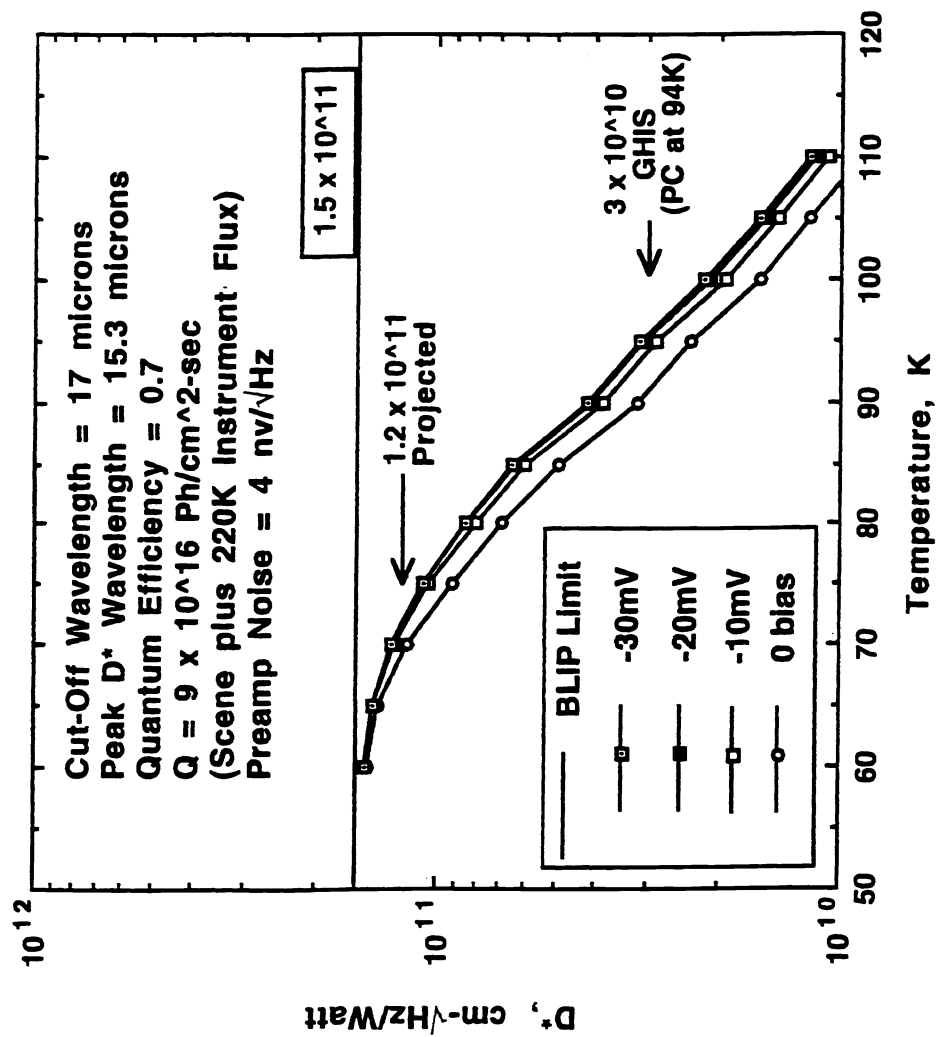


Figure 6. LW/PV D* vs. temperature and bias.

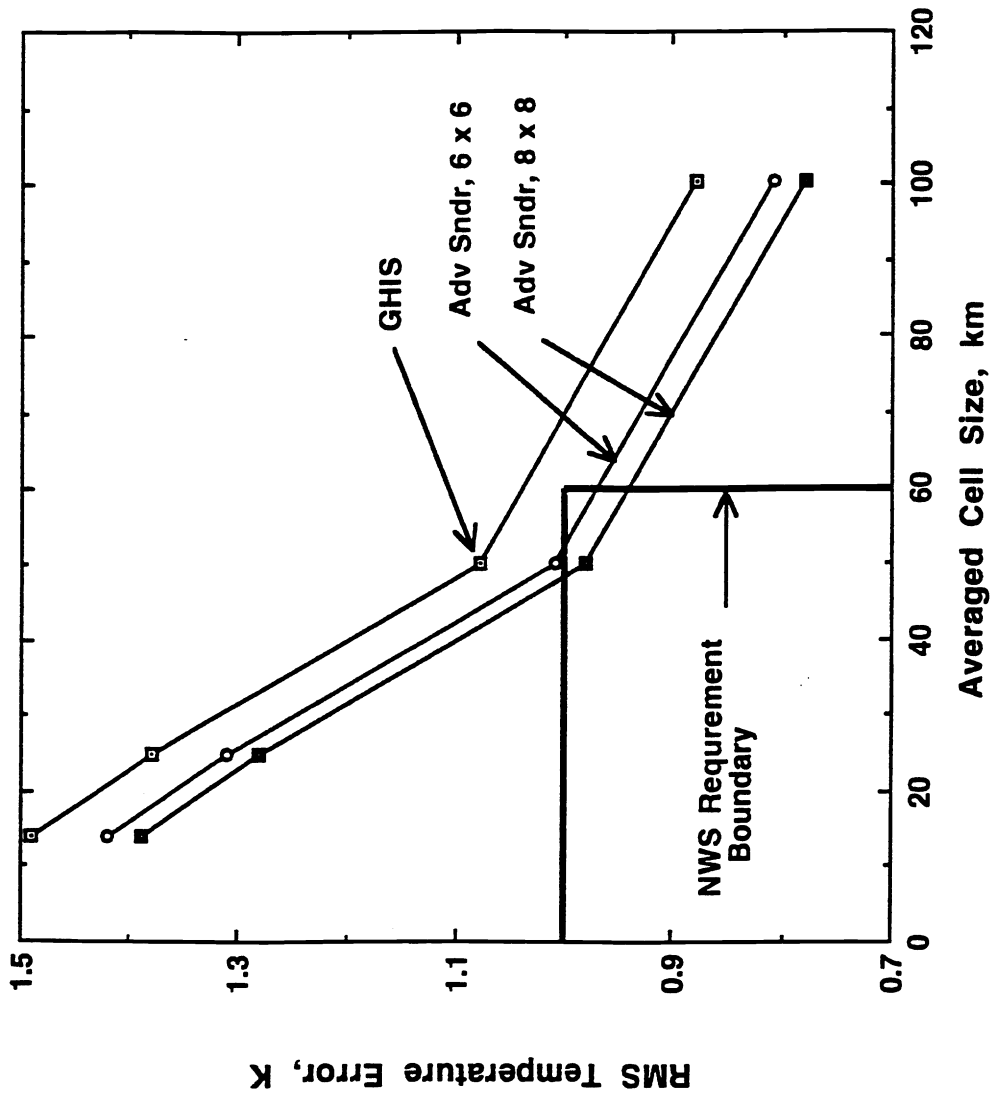


Figure 7. Estimated temperature retrieval performance (15 cm aperture, 65K FPA).